Optical properties of desert aerosol –I–

A. Tahiri [1], M. Diouri [1*], J. Barkani [2]

[1]*Atmospheric physics team (L.M.E), Faculty of science, University Mohamed First, Oujda, Morocco*
[2] *Laboratory of Engineering Sciences (LSI), Polydisciplinary Faculty of Taza, University Sidi Mohamed Ben Abdellah, Fez, Morocco*

Abstract

The desert aerosol plays a very important role in the atmospheric evolution as well as in the climate change. In this study, we present the results of the optical thickness, the single scattering albedo and radiative forcing of desert aerosol. These main optical parameters will be analyzed for six sites covering the main desert areas such as, Ouarzazate and Oujda (Morocco, North Africa), Tamanrasset (Algeria, North Africa), Dalanzadgad (Mongolia, Asia), Birdsville (Australia) and Frenchman-Flat (Nevada, West of United States). The annual cycle of the aerosol optical thickness daily averages shows variable values due to the changeable weather and the Sahara source. The maximum values were recorded at the Sahara site (Ouarzazate, 3.04; Tamanrasset, 2.76). The single scattering albedo daily averages ranges from 0.36 to 0.99 at Ouarzazate and Birdsville, and registers high proportional values at Oujda and Tamanrasset. The daily averages of Aerosol Radiatif Foricng at surface ranged from -375W/m^2 to -2W/m^2, being larger in spring and summer than in the rest of season. The seasonal ARF evolution was inconsistent with seasonal aerosol optical depth variation due to the effects induced by other aerosol parameter such as the single scattering albedo. The ARF at top of the atmosphere changed from +40 W/m^2 to -75 W/m^2. These results suggest that the Simpson dust caused local atmospheric heating over the Birdsville and also Saharan dust over Ouarzazate.

1. Introduction

The Sahara and the desert regions are the most important sources of terrestrial mineral dust, the latter being the main component of the atmospheric aerosol, in addition to the ocean aerosol and the anthropogenic aerosol, they act significantly and not yet sufficiently precise on global climate change. The Saharan desert covers an area of nearly 9 million km^2. It is the largest terrestrial desert that contributes to nearly 70% of annual global dust emissions. Dust storms are important sources of large particles. The atmospheric aerosol has a confirmed influence on the climate. Its direct effect on the latter is observed through the phenomena of diffusion and absorption of solar radiation. The indirect effect is manifested in the cloud formation process where the aerosols behave as condensation nuclei and modify the optical properties of the clouds. The mineral dust particles diffuse and absorb a portion of the solar radiation. In addition, because of the importance of the big-particle mode they contain, they modify the flux of the radiation on the surface of the earth. Mineral dust contributes to the warming of the atmosphere and has an impact on the hydrological cycle [1] and on the formation of ice clouds [2]. The temporal and spatial distribution of mineral dust is still uncertain in many regions of the world. The sign of the radiative forcing of these dusts at the top of the atmosphere is still uncertain [3]. Intensive and continuous observation at the global scale of the land is necessary to clarify its impact. This is done by satellites (Envisat, Modis, Terra, Aqua, Calipso, Parasol, Cloudsat) which are equipped with appropriate modules and photometers. The AERONET / PHOTONS network which makes ground recordings is a very important tool to study the optical properties of the atmospheric aerosol in several terrestrial regions and to validate satellite measurements [4] and [5]. Optical thicknesses of aerosols (AOT), single diffusion albedo (ω_0) and radiative forcing of the desert aerosol (ARF) are required to evaluate the influence of the latter on the regional and global radiative budget.

2. Materials and Methods
2.1 Geographical description of the stations (AERONET)

Of all the AERONET / PHOTONS stations (Aerosol Robotic NETwork / PHOtometry for Operational Processing of Satellite Normalization), we selected six stations taking into account their geographical location and the number of available data (Table 1). The six selected sites are located near the Sahara or in the main desert regions (Figure 1).

2.1.1 Oujda

Located at 620 m altitude and 55 km from the Mediterranean coast, it is bordered on the north by the Beni-Snassen Mountains. The solar photometer is located 10 meters from the ground at the faculty of science. The city of Oujda enjoys a dry climate with a cold winter less and less rainy, a warm summer with the influence of the desert air masses and rare showers. Precipitation is irregular with less than 400 mm per year. The average annual temperatures range from 15 °C to 20 °C. Maximum temperatures may exceed 40 °C (12 July 2011 with 45.7 °C), while minimum temperatures may be below 0 °C (28 January 2005 with -7.1 °C).
The city of Oujda knows during August the influence of the Chergui (hot wind of Saharan origin). (http://en.wikipedia.org/wiki/Oujda).

2.1.2 Ouarzazate

Is associated with the meteorological station. Ouarzazate is a small town with almost no industrial activity. It is located in the South-East of the Atlas and in the North-West of the Sahara. Ouarzazate has a pre-Saharan climate characterized by low rainfall and hot and dry climate, may be as Bsh Köppen classification. The average maximum temperature in July is 40 °C, the average minimum is 25 °C. In January, the minimum and maximum average temperatures are 2 °C and 16 °C respectively. At night, the temperature can drop to -4 °C. In the spring, clouds are rare and exceptional thunderstorms. The desert winds (Sirocco and Chergui) play an important role in the Ouarzazate climate (http://en.wikipedia.org/wiki/Orarazazate).

2.1.3 Tamanrasset

The photometer is installed on the roof of the regional meteorological center. This zone does not know any industrial activities and is located in the high plateaus of the Sahara. The climate of Tamanrasset is warm, sunny, arid and tropical, it is classified as BWh in Köppen classification. Winter temperatures are close to those of the rest of the Sahara, while the summer maximums are below 35 °C, the nights are icy and the days are mild. Tamanrasset is crossed by the Sirocco violent, very dry and very hot Saharan wind that blows over North Africa loaded with burning Saharan air mass. The Harmattan hot, dry and dusty wind of West Africa blows southward from the Sahara and is loaded with dust and sand.

2.1.4 Dalanzadgad

Is located at the top of a platform in southern Mongolia. The station is at an altitude of 1490 meters above sea level. Due to its high altitude and its remoteness from any sea, it has an extreme continental climate with BSk Köppen classification: very cold winter, with temperatures as high as -30 °C, and was short but hot, especially in the Gobi Desert. The sun shines on average 257 days a year, the country being generally at the center of a system of high pressures (anticyclones). It rains very little with an annual average of 250 mm in the North. The extreme south, Gobi desert may not receive rainfall for several years. (http://en.wikipedia.org/wiki/Dalanzadgad).

2.1.5 Birdsville

Is a village in Southeast Queensland in Australia, and boundary of South and the Simpson Desert. The solar photometer is installed near the maximum frequencies of dust storms. It lies just east of the Simpson Desert and north of the Strzelecki desert and receives prevailing winds from the South and West. The climate is very hot and dry in summer and cold in the Southeast area in winter with BWh of Köppen classification.

2.1.6 Frenchman-Flat

Is located in Nevada in the southwestern part of the United States. These are the desert lands in the shadow at the foot of the California Mountains of the Sierra Nevada. The landscape of Nevada is wrinkled by hundreds of mountainous intervals aligned parallel from North to South. Between these intervals are nested thousands of valleys of clay soil or sand or flat land of salt. The highest peaks and ridges of the mountains receive enough moisture. The climate of the desert tends to become very hot in summer and comfortable in autumn and spring and cooler in winter with BSh of Köppen classification.

Table 1: AERONET / PHOTONS studied stations

Station	Latitude (°)	Longitude (°)	Altitude (m)	year	Number of days (AOT)
Oujda	34.65	1.89	620	2015	216
Ouarzazate	30.92	6.91	1136	2015	338
Tamanrasset	22.79	5.53	1377	2015	342
Birdsville	25.89	139.34	46.5	2015	239
Dalanzadgad	43.57	104.41	1470	2014	325
Frenchman-Flat	36.80	115.93	940	2013	301
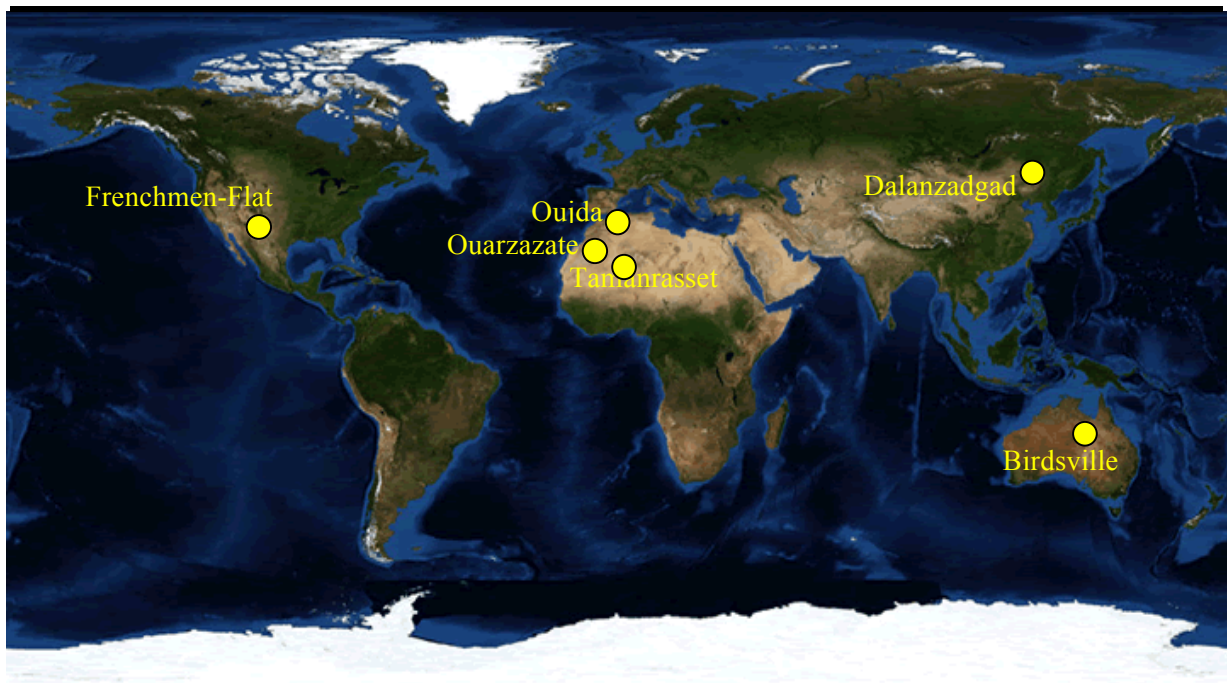
Figure 1: AERONET stations selected for the study of the desert aerosol

Table 2: Spectral corrections/components of wavelengths (μm)

Standard wavelengths (μm)	Version 1	Version 2
0,340 (0.002μm)	Rayleigh, O_3	Rayleigh, NO_2, O_3
0.380 (0.004μm)	Rayleigh	Rayleigh, NO_2
0.440 (0.010μm)	Rayleigh	Rayleigh, NO_2
0.500 (0.010μm)	Rayleigh, O_3	Rayleigh, NO_2, O_3
0.675 (0.010μm)	Rayleigh, O_3	Rayleigh, O_3
0.870 (0.010μm)	Rayleigh	Rayleigh
1.020 (0.010μm)	Rayleigh	Rayleigh, H_2O
1.640 (0.025μm)	Rayleigh	Rayleigh, H_2O, CO_2, CH_4

Figure 2: Solar photometers CIMEL CE-318 installed at the six sites

2.2 Solar photometer methods

The AERONET / PHOTONS network was set up by the Goddard Space Flight Center (NASA, USA) and the Atmospheric Optics Laboratory of Lille (CNRS, France) in 2003. Since its creation, it has collected ground measurements by solar photometers to specify the optical and microphysical properties of the particles contained in the atmosphere. Since the establishment of this network, data are available on the internet site (http://aeronet.gsfc.nasa.gov/) about 1000 stations spread all over the globe, are currently listed. The instruments of the network are regularly checked and calibrated with an identical protocol. The data are processed in the

same way regardless of the date and place of acquisition, whether for the inversion itself [6] or for the rejection of the measurements affected by the presence of clouds [7]. The CIMEL CE-318 solar photometers (Figure 2) are instruments allowing the restitution of the optical and microphysical properties of vertically integrated aerosols of the atmospheric column. Photometric measurements are possible only during the day when the sun is visible and in the absence of clouds. The automated photometer is produced by the French company CIMEL electronics. It is developed in France by the Laboratory of Atmospheric Optics (Lille). Its detailed description is made by B. Holben et al., 1998 [8]. The photometer is equipped with a robot with two axes allowing movements in the zenith and azimuth planes and can aim at any point of the celestial cost with an accuracy of 0.05° and a field of view of 1.2°. It has a filter wheel to measure in eight channels between 0.34 and 1.64 μm. The basic wavelengths are 0.34; 0.38; 0.44; 0.50; 0.675; 0.87; 1.02 and 1.64 μm (Table 2). These spectral filters with a width of 0.01 μm correspond to atmospheric windows where the absorption of solar radiation by the gaseous compounds is low. The data is transmitted by a geostationary satellite every four hours to a single processing center located at NASA's Goddard Space Flight Center. The photometer provides direct sunlight measurements and scattering measurements according to the angular luminance distribution of the sky ($W/m^2.Sr.\mu m$) in the Almucantar (circle of the same solar elevation including the sun and which forms the base of the half angle cone the constant zenith angle of view θ, (Fig. 3). Several sequences of Almucantar measures in average in 35s are carried out morning and afternoon. A sequence of measurements records i measurements along the Almucantar A_i directions on 2π (rd).

There are different levels of data processing available: level 1 (raw data), level 1.5 (the cloud mask is automatically applied when the final calibration is not necessarily performed) and level 2 (the cloud mask is applied as well than the final calibration). For our study, the data for levels 1.5 and 2 were used.

The algorithm used in AERONET [6] and [9] characterizes aerosols by assimilating luminance simulated by a radiative transfer code with measurements of luminance (direct luminance of the sun and sky luminance) obtained at 4 wavelengths (0.44, 0.675, 0.87 and 1.02μm). The radiative transfer is related to the refractive (and wavelength-dependent) indices of the aerosols and their distribution. The use of this radiative transfer code makes it possible to determine by inversion the desired optical properties with a minimum of starting hypotheses (spherical particles, homogeneous and distributed log-normal). Several studies with other radiative transfer codes involving non-linear inversion methods have been carried out [10] and [11] and have allowed the determination of the optical properties of the desert aerosol. The last ones [12] have been proposed for particles of non-spherical shapes.

In our study, the data are obtained from the measurements of six solar photometric stations (Table 1; Figure 1) of the AERONET / PHOTONS network. The data considered represent the optical and radiative parameters of aerosols: optical thickness AOT which can be written also (τ_a), single scattering albedo (ω_0) and aerosol radiative forcing (ARF). The available AOT data for the six stations is automatically provided according to the standard AERONET wavelengths (Table 2).

3. Results

3.1 Aerosol Optical Thickness

Aerosols are small solid or liquid particles suspended in the atmosphere. They come from natural or anthropogenic sources and their size can vary from nanometer (groups of molecules) to a few tens of micrometers (dust particles). Since the industrial revolution, man began to emit massively aerosols. Alongside natural Ocean and desert emissions, the most aerosol-producing sectors are transport, agricultural erosion and forest fires.

The optical thickness of the aerosol, denoted $\tau_a (\lambda)$ is dimensionless, it quantifies the extinction of the incident radiation in a column of atmosphere, both by absorption and by diffusion. $\tau_a (\lambda)$ is a very important physical parameter for the characterization of aerosols, it gives an indication of the content of atmospheric aerosols. The study of the annual evolution of the AOT allows us to analyze the changes in the type of aerosol as well as its concentration between the different seasons. The optical thicknesses of aerosols can reach very high values for sand storms, it is common to observe optical thicknesses of aerosols at 0.5 μm exceeding 2 that can go beyond 4

to the African continent [13]. The technique for direct measurement of the optical thickness of the aerosol is the measurement of the attenuation by the atmosphere of direct solar radiation. The decrease of the solar flux is expressed by the Bouguer law:

$$I(\lambda) = I_0(\lambda)e^{-m_{air}\tau(\lambda)} \tag{1}$$

With τ (λ) total optical thickness which accounts for the contribution to the attenuation of aerosols, Rayleigh scattering and atmospheric gases.

$$\tau(\lambda) = \tau_a(\lambda) + \tau_{Ray}(\lambda) + \tau_{gaz}(\lambda) \tag{2}$$

$$\tau_a(\lambda) = \frac{1}{m_{air}}\ln\left(\frac{I_0(\lambda)}{I(\lambda)}\right) - \tau_{Ray}(\lambda) - \tau_{gaz}(\lambda) \tag{3}$$

$$m_{air} = \begin{cases} (\cos(\theta))^{-1} & si \ \theta \leq 75° \\ [(\cos(\theta) + a(b-\theta)^{-c})]^{-1} & si \ \theta \geq 75° \\ a = 0.50572, \quad b = 83.92005°, \quad c = 1.6364 \end{cases} \tag{4}$$

$$\tau_{Ray}(\lambda) = \frac{p}{p_0}0.00877.\lambda^{-4.05} \tag{5}$$

With:
I (λ): solar flux measured by the solar photometer (W / m^2)
I$_0$ (λ): extra-terrestrial solar flux (W / m^2)
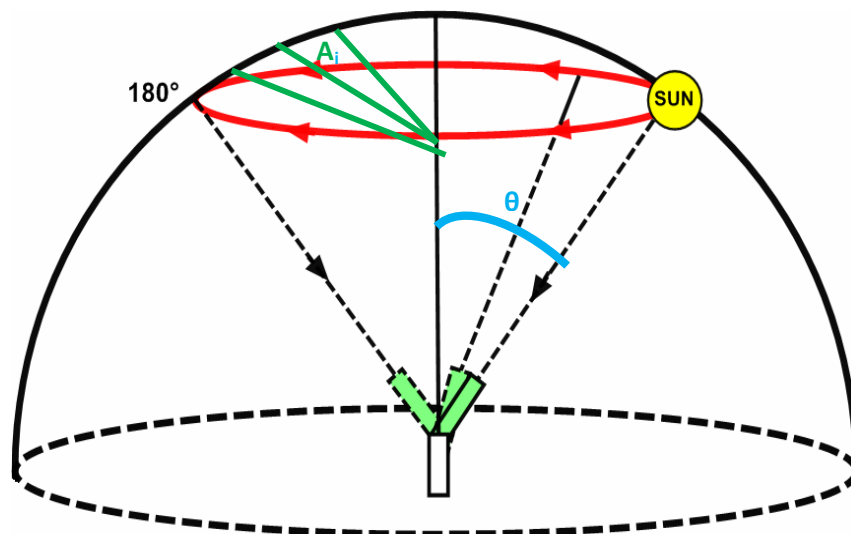
Figure 3: Solar photometer in position ALMUCANTAR

In Oujda (Fig.4.a), the annual cycle of the aerosol optical thickness shows peaks in spring and summer, which coincide with the activity of dust production in southeastern Morocco. The annual cycle can be divided into two periods: the first one spreads from March to September with high AOT values and significant differences between the daily averages recorded for 0.5 μm. The second period from October to February with low values and small discrepancies observed between these months. The values observed for these two seasons confirm the importance of desert aerosol in summer and less degree in spring, in line with previous measurements in 2000, 2001, 2005 and 2015 by some researchers [14-17].
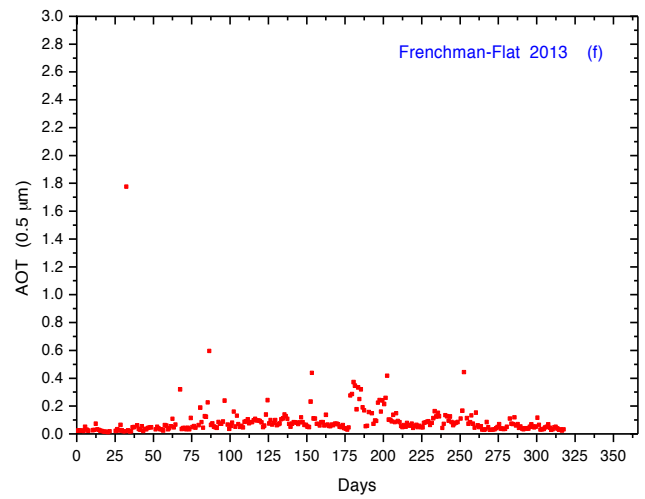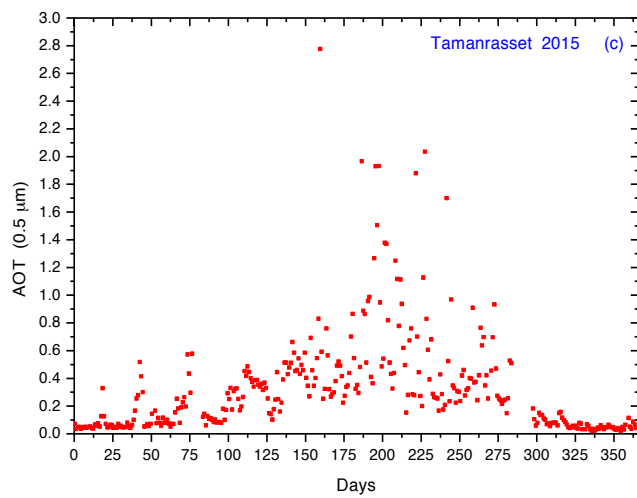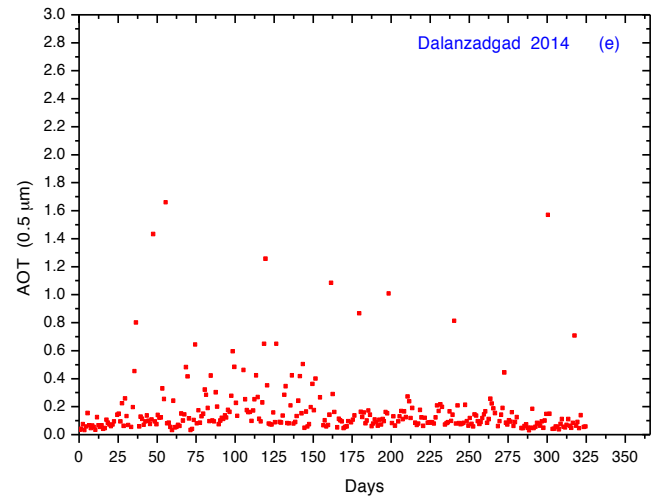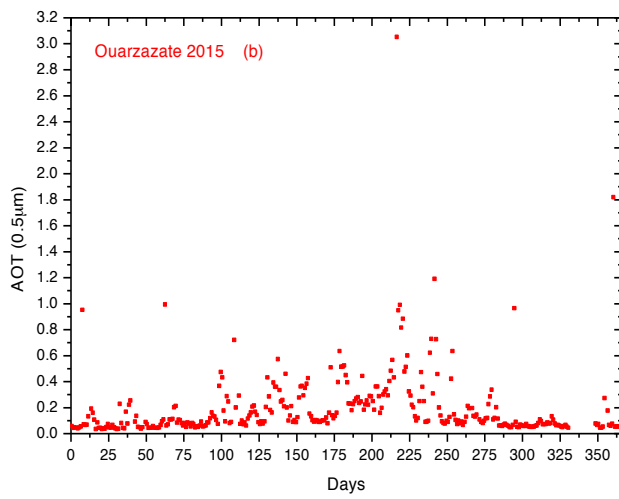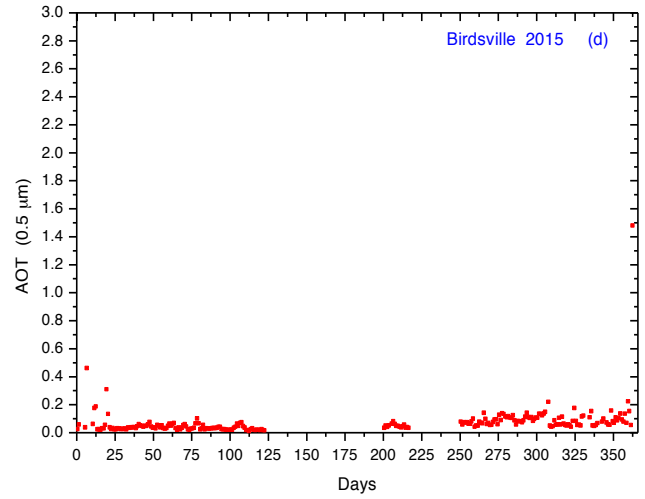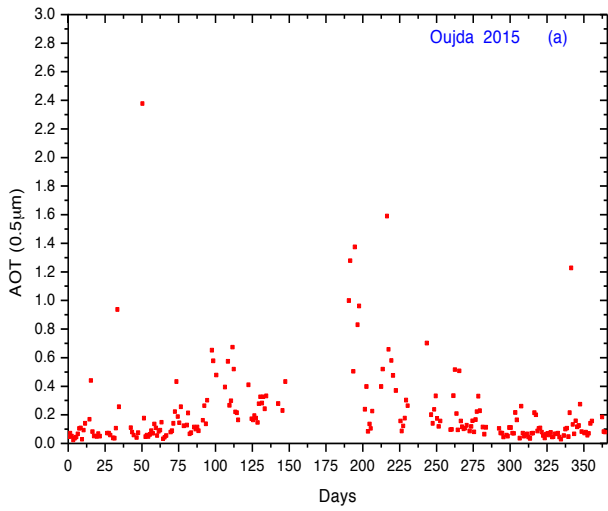
Figure 4: Daily means of AOD (λ = 0.5 μm) for Oujda (a), Ouarzazate (b), Tamanrasset (c), Birdsville (d), Dalandzadgad (e) and Frenchman-Flat (f)

In Ouarzazate (Fig.4.b), peaks are recorded in spring and summer. The aerosol type changes alternately in the Ouarzazate region because of the low influence associated with the Atlantic air masses which moderate the dust load of the East and Saharan air masses (summer). Minimum values are recorded in the fall and winter. During the SAMUM experimental measurement campaign carried out in May-June 2006 in Ouarzazate, the average daily AOT in May-June 2006 for the 0.5 μm wavelength is 0.28 [18], in agreement with the AERONET data (Fig.4.b).

The annual cycle of daily AOT averages for Tamanrasset (Fig.4.c) shows strong variability recorded for the large values (from March to September) with a maximum value of 2.76. Very high values are characteristic of the Saharan aerosol charge, and are practically within Saharan sources. While, the low variability of the AOT coincide with low values observed between October and February. These low values are characteristic of fine particles. Similar results have been reported by Kim et al. [19] with analysis limited to the properties of dust aerosols with data (AOD ≥ 0.4) and Angstrom coefficients less than 0.2.

The Birdsville site (Fig.4.d) records very low values of the daily averages during 2013 with a maximum in February (~ 1.47) due to the influence of the Simpson Desert and the presence of long dune bands (red sand).

For the Dalanzadgad region (Fig.4.e), the annual cycle records values below 0.3 and peaks are observed in March-April-May with a value of ~ 1.65. These peaks are due to the influence of the sand dunes of the Gobi Desert which is located between northern China and southern Mongolia. The AOT values show significant variations throughout the year, characteristics of submicron particles. These values are due to the diversity of the landscapes of the Dalanzadgad which consists of vast plains, imposing mountain ranges and sand dunes, as well as saline steppe areas. In Dalanzadgad, the sun shines about 250 days a year.

A Frenchman-Flat (Fig.4.f) shows a relatively low variability between the different seasons of the year 2013 and less than 0.2. The Frenchman-Flat region is influenced by aerosols from flat salt and sand fields.

Table 3: Annual Averages, Minimum and Maximum AOT

Site	Annual. A (AOT)	Minimum (AOT)	Maximum (AOT)
Oujda	0.21 ± 0.28	0.01	2.37
Ouarzazate	0.19 ± 0.26	0.03	3.04
Tamanrasset	0.32 ± 0.37	0.02	2.76
Birdsville	0.06 ± 0.10	0.007	1.47
Dalanzadgad	0.16 ± 0.21	0.02	1.65
Frenchman-Flat	0.08 ± 0.12	0.007	1.76

3.2 Single Scattering Albedo

The single scattering albedo (ω_0) is one of the optical parameters that accounts for the importance of diffusion in estimating the radiative impacts of aerosols. (ω_0) corresponds physically to the ratio between the diffusion cross section (σ_d) and the extinction cross section (σ_e) of a particle, it translates the probability that the photons intercepted by the aerosol particle are diffused and it is defined by:

$$\omega_0 = \frac{\sigma_d(\lambda)}{\sigma_e(\lambda)} = \frac{\sigma_d(\lambda)}{\sigma_d(\lambda) + \sigma_a(\lambda)} \qquad (6)$$

Where σ_a is the absorption cross-section of aerosol.

The more absorbing the aerosol, the larger the imaginary part of the refractive index and the smaller ω_0. For a non-absorbing aerosol (imaginary part of the index of refraction equal to 0), ω_0 is equal to 1. The absorption properties are directly related to the chemical composition of the aerosol and to its refractive index.

The single scattering albedo ω_0 is the ratio of the diffuse radiation to the total extinction radiation. It is a key variable to evaluate the radiative effects of aerosols [20]. The influence of aerosols on climate change is confirmed. Dubovik et al. [2006] were able to determine the ω_0 for ground measurements of the global AERONET network [21]. Several studies on the variations of the single scattering albedo ω_0 of the aerosols have been carried out. For example, Eck et al. [1999] from the spectral dependence have indicated that the values of ω_0 of 0.70 to 0.92 are for aerosols of biomass fires and 0.70 to 0.99 for desert dust particles [22].

Masmoudi et al. [2003], analyzing the variation of the ω_0 of the photometric stations in Africa, indicated that ω_0 increases with the wavelength for different optical thicknesses of the aerosols and that the African regions are particularly affected by the particles of dust [23]. In the literature, there is a wide range of ω_0 values for desert dust. Using a combination of satellite (Landsat TM) and photometric (AERONET) measurements, D.Tanré et al [24] obtained a ω_0 value for Saharan dust (0.97 ± 0.02 to 0.55 μm on average over the atmospheric column) close to that obtained by Dubovik et al.[20] for the Persian Gulf (0.93 ± 0.03 to 0.44 μm). These values are in good agreement with those obtained on the surface by [25] $\omega_0 = 0.95$; 0.97 for 0.66 μm from direct measurements of diffusion (nephelometer) and absorption (aethalometer) of solar radiation by mineral particles from the Gobi Desert, the Sahara and the Sahel region. Values of ω_0 in the visible range from 0.75 to 0.95 were measured by Otto et al.[26] and Slingo et al. [13] and were equal to 0.99 McConnel et al.[27] and Osborne et al.[28]. For this study, the values of ω_0 obtained are high in the neighborhood of 0.9, Table 4.a average in agreement with that obtained by the various authors presented in Table 4.b

Table 4.a: Single scattering albedo ω_0 of the sites studied

Site	Annual. A	Minimum	Median	Maximum
Oujda	0.83 ± 0.08	0.53	0.85	0.98
Ouarzazate	0.68 ± 0.14	0.36	0.70	0.99
Tamanrasset	0.87 ± 0.09	0.36	0.89	0.98
Birdsville	0.72 ± 0.19	0.40	0.84	0.98
Dalanzadgad	0.85 ± 0.07	0.62	0.86	0.99
Frenchman-Flat	0.87 ± 0.08	0.58	0.88	0.99

Table 4.b: Single scattering albedo ω_0 of the desert aerosol

References	ω_0	λ (μm)
Müller et al, 2011 [29]	0.96	0.550
Johnson and Osborne, 2011 [30]	0.97 ± 0.02	0.550
W von Hoyningen-Huene et al, 2009 [4]	0.93 at 0.98	0.753
McFarlane et al, 2009 [31]	0.99	0.500
Schladitz et al, 2009 [32]	0.96 ± 0.02	0.537
Otto et al, 2009 [33]	0.79	0.532
Raut and Chazette, 2008 [34]	0.90-0.92	0.440
Osborne et al, 2008 [28]	0.98-0.99	0.550
Levy et al, 2007 [35]	0.953	0.550
Otto et al, 2007 [36]	0.75-0.76	0.550
Slingo et al, 2006 [13]	0.89-0.95	0.500
Dubovik et al, 2002 [20]	0.93	0.440

The site of Ouarzazate (Fig.5.b) presents a wide range of variation (0.36-0.90) relative to the polydispersion of the particles of the Saharan source and to the influence of the Atlantic advections. For the other sites (Fig.5.a,c,d,e,f) the variation is small and can be explained by the distance of the source which leads to a monodispersion effect of the particles supported by the meteorological evolution conditions.

3.3 Aerosol Radiative Forcing

The aerosol radiative forcing (expressed in W/m^2) is defined as the difference of the net radiative flux resulting from the presence of aerosols (Equation 7). It can be quantified at the top of the atmosphere (z at the top of the TOA atmosphere) or at the ground surface (z at the BOA surface). A positive radiative forcing tends to warm the terrestrial system, negative tends to cool it :

$$\Delta F_z = \left(F^{\downarrow} - F^{\uparrow} \right) - \left(F^{\downarrow 0} - F^{\uparrow 0} \right) \qquad (7)$$

By distinguishing the flux $F^{\uparrow}$ (visible + infrared) rising and the flow $F^{\downarrow}$ (visible + infrared) descending. The indices ($^{\uparrow 0}$) and ($^{\downarrow 0}$) correspond to the fluxes calculated without aerosol, the case of the very clear sky. A clean

aerosol-free atmosphere is characterized by a maximum of global irradiance, a minimum of diffuse irradiance and optical thicknesses very close to zero.
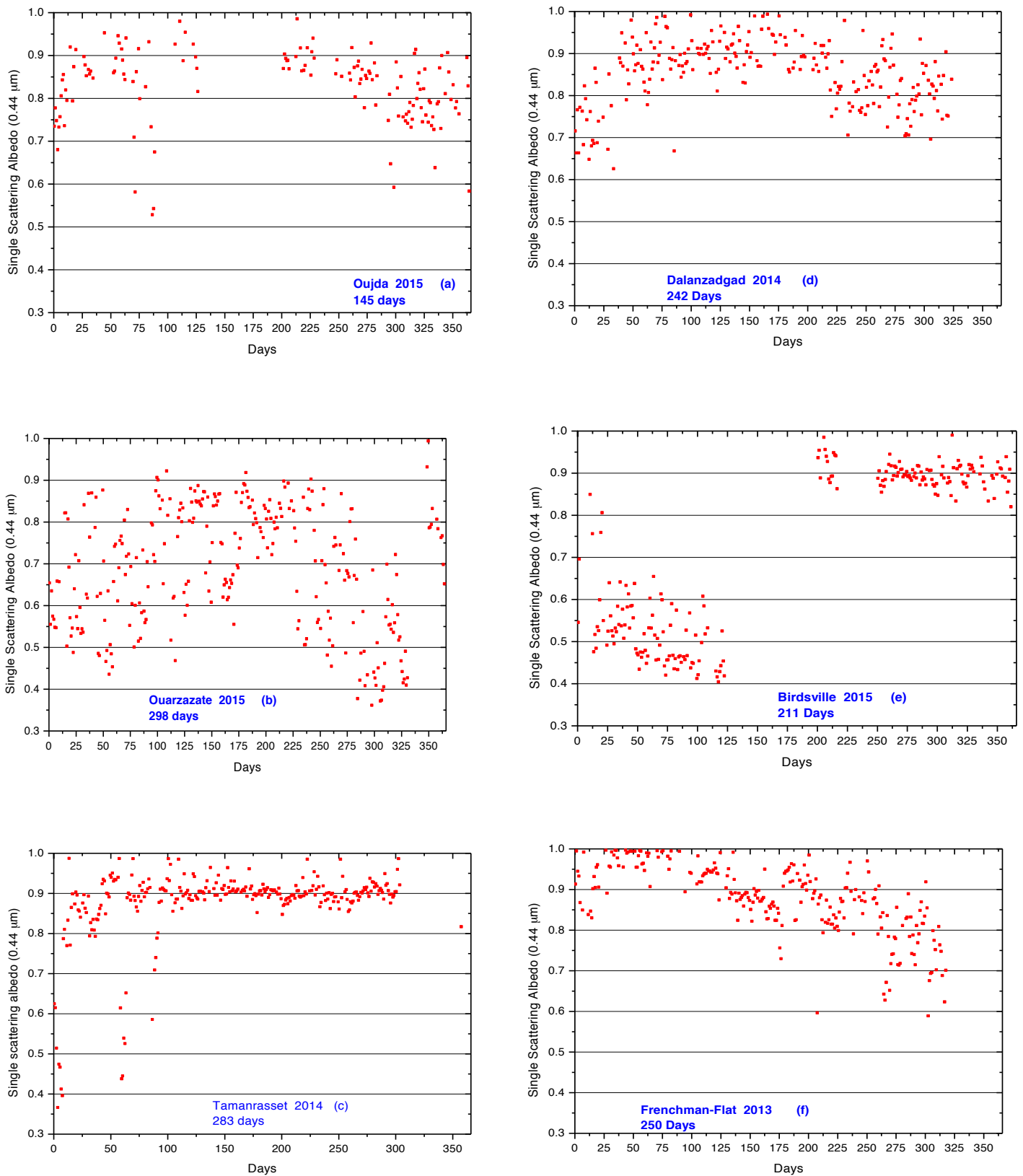
Figure 5: Daily averages of the single scattering albedo (ω_0)

The radiative forcing of the aerosols depends on the intrinsic properties of the aerosol, particularly its composition and its distribution in particle size but also on the relative humidity of the air as well as the surface albedo of the soil. At the top of the atmosphere, for the large particles mode, the effects of the Mie diffusion are subtractive, while on the surface these effects are additive [37]. For purely diffusing aerosols, direct radiative forcing at the top of the atmosphere is close to 0 and negative on the surface. Desert aerosols and certain organic carbons transfer the energy absorbed by an adiabatic heating of their environment (positive atmospheric radiative forcing) [38]. In this case, radiative forcing at the surface can be two to three times greater than that exerted at the top of the atmosphere [39].

In North Africa, the values of the daily averages of the aerosol radiative forcing for Oujda, Ouarzazate and Tamanrasset (Fig. 6.a, b, c) observed at the land surface in 2014 (2015), 375 W/m^2 and -5 W/m^2 with minimum values observed in spring and summer and peaks recorded with minimum values -178 W/m^2 (Oujda), -303 W/m^2 (Ouarzazate), -375 W/m^2 (Tamanrasset). The most important values are recorded in the Sahara (Tamanrasset). These values confirm the importance of the large-particle mode characteristic of the aerosol of regional desert storms observed in spring and summer.

For figure 6, (d. e. f), the ARF values show small monthly variations between -1.13 W/m^2 and -98.89 W/m^2 with small differences between sites. Low values show a smaller fraction of coarse particles, as the deserts of Australia (Birdsville), Mongolia (Dalanzadgad) and Nevada (Frenchman-Flat) have low influences of dust emissions into the atmosphere, the Sahara in North Africa has strong influences.
The values of the daily averages of the ARF at the top of the atmosphere for the six sites (Fig. 6) are variable between +38 W/m^2 and -79 W/m^2 and are located in the vicinity of 0 W/m^2 on the whole of the field of our study except for a few days, we see passages from negative values to positive values, explained by the greater amount of available radiative energy that was reflected by the passenger clouds.

Table 5.a: Aerosol Radiative forcing of the sites studied

Site	ARF (BOA) (W/m^2)			ARF (TOA) (W/m^2)		
	Mean	Minimum	Maximum	Mean	Minimum	Maximum
Oujda	-26.03 ± 19.09	-178.95	-6.14	-3.21 ± 7.82	-59.74	15.63
Ouarzazate	-41.74 ± 25.63	-303.72	-9.66	1.35 ± 9.64	-71.72	18.69
Tamanrasset	-42.91 ± 39.77	-375.08	-5.27	-6.43 ± 12.13	-78.97	26.57
Dalanzadgad	-25.28 ± 13.91	-98.89	-6.72	-6.61 ± 8.07	-45.91	5.59
Birdsville	-24.85 ± 14.96	-82.40	-3.51	6.53 ± 9.47	-8.77	37.42
Frenchman-Flat	-14.02 ± 9.18	-63.80	-1.13	0.97 ± 3.82	-18.53	30.57

Table 5.b: Radiative forcing of the desert aerosol

References	ARF (BOA) (W/m^2)	ARF (TOA) (W/m^2)	Sites and pays
Garcia et al, 2011 [40]	-88 ± 41	-38 ± 18	Region centrale d'Afrique
Perrone et al, 2011 [41]	-53 ; -25	-25; -11	Lecce, Italy
Mallet et al, 2009 [42]	-137.83	-11.83	Modele regional Mean (Sahel)
Derimian et al, 2008b [43]	-29.1	-8.1	M'Bour, Senegal
Yoshioka et al, 2007 [44]	-9.07	-5.85	Afrique du Nord
Meloni et al, 2005 [45]	-11 ; -14.2	-5.1; -8.7	Lampedusa, Italy
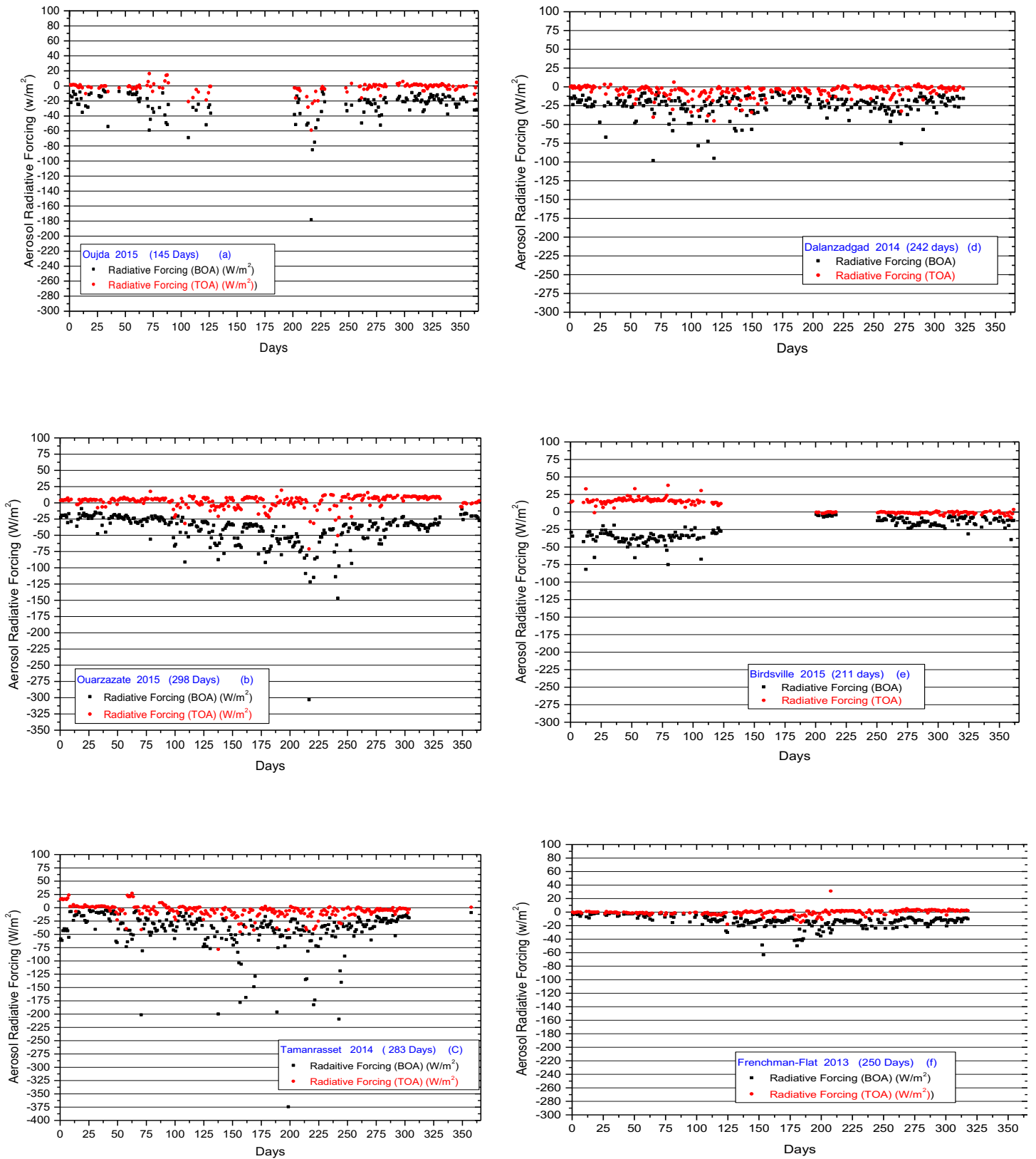
Figure 6: Daily averages of the Aerosol Radiative Forcing at the surface (BOA) and at the top of the atmosphere (TOA)

Conclusion

Daily averages of the desert aerosol optical thicknesses obtained at Tamanrasset, Saharan source, confirm its influence with relatively high values near 0.3 observed mainly in summer. Oujda and Ouarzazate have more than three seasons where daily averages vary above 0.2. The other sites show a low variability with annual average near 0.07. The single scattering albedo varies between 0.7 and 0.87 while remaining relatively lower than the one cited by the literature always greater than 0.9 in mean.

The aerosol radiative forcing appear to be relatively constant at the top of the atmosphere, near 0 W/m^2 in mean and around -30 W/m^2 on the land surface. Sites in North Africa Oujda and Ouarzazate show a more marked summer period especially in Ouarzazate where it can reach -303 W/m^2 at surface.

References

1. R. L. Miller, J. Perlwitz, I. Tegen, *J. Geophys. Res. Atmos.,* 109 (2004) 1-24.

2. A. Ansmann, I. Mattis, D. Müller, U. Wandinger, M. Radlach, D. Althausen, R. Damoah, *J. Geophys. Res. Atmos.,* 110 (2005) 1-12.

3. J. Haywood, O. Boucher, *Rev. Geophys.,* 38(4) (2000) 513-543.

4. W. von Hoyningen-Huene, T. Dinter, A. A. Kokhanovsky, J. P. Burrows, M. Wendisch, E. Bierwirth, D. Müller, M. Diouri, *Tellus B*, 61(1) (2009) 206-215.

5. T. Dinter, W von Hoyningen-Huene, J. P. Burrows, A. Kokhanovsky, E. Bierwirth, M. Wendisch, D. Müller, R. Kahn, M. Diouri, *Tellus B*, 61(1) (2009) 229-238.

6. O. Dubovik, A. Smirnov, B. N. Holben, M. D. King, Y. J. Kaufman, T. F. Eck, I. Slutsker, *J. Geophys. Res. Atmos.,* 105 (2000) 9791-9806.

7. A. Smirnov, B. N. Holben, T. F. Eck, O. Dubovik, I. Slutsker, *Remote Sens. Environ.,* 73(3) (2000) 337-349.

8. B. N. Holben, T. F. Eck, I. Slutsker, D. Tanré, J. P. Buis, A. Setzer, E. Vermote, J. A. Reagan, Y. J. Kaufman, T. Nakajima, F. Lavenu, I. Jankowiak, A. Smirnov, *Remote Sens. Environ.,* 66 (1) (1998) 1-16.

9. O. Dubovik, M. D. King, *J. Geophys. Res. Atmos.,* 105(2000) 20673-20696.

10. M. Diouri, S. I. Sanda, CLEOPATRE-I code, *J. Aerosol Sci.,* 28 (1997) S459.

11. M. Wendisch, W. von Hoyningene-Huene, *Atmos Environ.*, 28 (5) (1994) 785-792.

12. M.I. Mishchenko, L.D. Travis, A.A. Lacis, A.A, *Cambridge University Press*, New York (2006).

13. A. Slingo, T. P. Ackerman, R. P. Allan, E. I. Kassianov, S. A. McFarlane, G. J. Robinson, J. C. Barnard, M. A. Miller, J. E. Harries, J. E. Russell, S. Dewitte, *Geophys. Res. Lett.,* 33 (2006) L24817.

14. L. El Amraoui, M. Diouri, *J. Aerosol Sci.*, 32(1) (2001) S643-S644.

15. L. El Amraoui, M. Diouri, M. El Hitmy, R. Jaenicke, L. Schütz, W.von Hoyningen-Huene, *J. Aerosol Sci.*, 31(1) (2000) S277- S278.

16. I. El Aouadi, *Thèse de Doctorat* de l'Université Mohamed Premier (Maroc) (2005) 55-64.

17. A. Tahiri, *Thèse de Doctorat* de l'Université Mohamed Premier (Maroc) (2015) 67-68.

18. C. Toledano, M. Wiegner, M. Garhammer, M. Seefeldner, J. Gasteiger, D. Muller, P. Koepke, *Tellus B, 61* (2009) 216-228.

19. D. Kim, M. Chin, H. Yu, T.F. Eck, A. Sinyuk, A. Smirnov, B. N. Holben, *Atmos. Chem. Phys.*, 11 (2011) 10733-10741.

20. O. Dubovik, B.N. Holben, T.F. Eck, A. Smirnov, Y. J. Kaufman, M. D. King, *J. Atmos. Sci.*, 59 (2002) 590-608.

21. O. Dubovik, A.Sinyuk, T. Lapyonok, B.N. Holben, M. Mishchenko, P. Yang, T.F. Eck, H. Volten, O. Munoz, B. Veihelmann, W. J. van der Zander, M. Sorokin, I. Slutsker, *J. Geophys Rese Atmos.*, 111 (2006) 208.

22. T. F. Eck, B. N. Holben, J. S. Reid, O. Dubovik, A. Smirnov, N. T. O'Neill, I. Slutsker, S. Kinne, *J. Geophys. Res.*, 104 (1999) 31333-31349.

23. M. Masmoudi, M. Chaabane, D. Tanré, P. Gouloup, L. Blarel, F. Elleuch, *Atmos. Res.*, 66 (2002) 1-19.

24. D. Tanré, Y. J. Kaufman, B. N. Holben, B. Chatenet, A. Karnieli, F. Lavenu, L. Blarel, O. Dubovik, L. A. Remer, A. Smirnov, *J. Geophys. Res.*, 106 (2001) 18205-18217.

25. S.C. Alfaro, S. Lafon, J.L. Rajot, P. Formenti, A. Gaudichet, M. Maille, *J. Geophys. Res.*, 109 (2004) d08208.

26. S. Otto, M. de Reus, T. Trautmann. A. Thomas. M. Wendisch, S. Borrmann, *Atmospheric Chem. Phys.,* 7(18) (2007) 4887-4903.

27. C. L. McConnell, E. J. Highwood, H. Coe, P. Formenti, B. Anderson, S. Osborne, S. Nava, K. Desboeufs, G. Chen, M. A. J. Harrison, *J. Geophys. Res.*, 113 (2008) d14S05.

28. S. R. Osborne, T. Johnson, J. M. Haywood, A. J. Baran, M. A. J. Harrison, C. L. McConnell, *J. Geophys. Res.*, 113 (2008) d00C03.

29. T. Müler, A. Schladitz, K. Kandler, A. Wiedensohler, *Tellus B*, 63(4) (2011) 573-588.

30. T. B. Johnson, R.S. Osborne, *Q. J. Royal Meteorol. Soc.,* 137 (658) (2011) 1117-1130.

31. A. S. McFarlane, L. E. Kassianov, J. Barnard, C. Flynn, P.T. Ackerman, *J. Geophys. Res.*, 114 (2009) 65.

32. A. Schladitz, T. Müler, N. Kaaden, A. Massling, K. Kandler, M. Ebert, *Tellus B*, 61(1) (2009) 64-78.

33. S. Otto, E. Bierwirth, B. Weinzierl, K. Kandler, M. Esselborn, M. Tesche, A. Schladitz, M. Wendisch, T.Trautmann, *Tellus B*, 61(1) (2009) 270-296.

34. J. Raut, P. Chazette, *Atmospheric Chem. Phys.*, 8(22) (2008) 6839-6864.

35. R.C. Levy, L.A. Remer, O. Dubovik, *J. Geophys. Res.*, 112 (D13) (2007) D13210.

36. S. Otto, M. de Reus, T. Trautmann, A. Thomas, M. Wendisch, S. Borrmann, *Atmospheric Chem. Phys.*, 7(18) (2007) 4887-4903.

37. M. Iqbal, An Introduction to Solar Radiation, *Academic Press*, Toronto (1983).

38. Y. Derimian, A. Karnieli, Y. J. Kaufman, M.O. Andreae, T. W. Andreae, O. Dubovik, W. Maenhaut, I. Koren, *Chem. Phys.*, 8(13) (2008) 3623-3637.

39. S.K. Satheesh, V. Ramanathan, *Nature*, 405 (2000) 60-63.

40. E.O. Garcia, F. J. Exposito, P.J. Diaz, M.A. Diaz, *J. Geophys. Res.*, 116 (2011) D0120.

41. R. M. Perrone, A. Bergamo, *Atmospheric Res.*, 101 (2011) 783-798.

42. M. Mallet, P. Tulet, D. Serca, F. Solmon, O. Dubovik, J. Pelon, *Atmospheric Chem. Phys.,* 9 (2009) 2967-3006.

43. Y. Derimian, F. J. Léon, O. Dubovik, I. Chiapello, D. Tanré, A. Sinyuk, F. Auriol, T. Podvin, G. Brogniez, B. N. Holben, *J. Geophys. Res.*, 113 (2008) 47.

44. M. Yoshioka, M.N. Mahowald, J.A. Conley, D.W. Collins, W.D. Fillmore, S. C. Zender, *J. Clim*, 20 (2007) 1445-1467.

45. D. Meloni, A. di Sarra, T. Di Iorio, G. Fiocco, *J. Quant. Spectrosc. Radiat. Transfer*, 93 (2005) 397-413.

(2018) ; http://www.jmaterenvironsci.com